

University of Groningen

OmegaCAM and gravitational lensing

Christen, Fabrice Frédéric Thiébaud

IMPORTANT NOTE: You are advised to consult the publisher's version (publisher's PDF) if you wish to cite from it. Please check the document version below.

Document Version

Publisher's PDF, also known as Version of record

Publication date:

2007

[Link to publication in University of Groningen/UMCG research database](#)

Citation for published version (APA):

Christen, F. F. T. (2007). *OmegaCAM and gravitational lensing*. s.n.

Copyright

Other than for strictly personal use, it is not permitted to download or to forward/distribute the text or part of it without the consent of the author(s) and/or copyright holder(s), unless the work is under an open content license (like Creative Commons).

The publication may also be distributed here under the terms of Article 25fa of the Dutch Copyright Act, indicated by the "Taverne" license. More information can be found on the University of Groningen website: <https://www.rug.nl/library/open-access/self-archiving-pure/taverne-amendment>.

Take-down policy

If you believe that this document breaches copyright please contact us providing details, and we will remove access to the work immediately and investigate your claim.

Downloaded from the University of Groningen/UMCG research database (Pure): <http://www.rug.nl/research/portal>. For technical reasons the number of authors shown on this cover page is limited to 10 maximum.



RIJKSUNIVERSITEIT GRONINGEN

OmegaCAM and Gravitational Lensing

Proefschrift

ter verkrijging van het doctoraat in de
Wiskunde en Natuurwetenschappen
aan de Rijksuniversiteit Groningen
op gezag van de
Rector Magnificus, dr. F. Zwarts,
in het openbaar te verdedigen op
vrijdag 27 april 2007
om 16.15 uur

door

Fabrice Frédéric Thiébaud Christen

geboren op 5 april 1974
te Mulhouse, Frankrijk

Promotores:

Prof. dr. K.H. Kuijken
Prof. dr. E.A. Valentijn

Beoordelingscommissie:

Prof. dr. P.D. Barthel
Prof. dr. R.F. Peletier
Prof. dr. E. Tolstoy

ISBN 978-90-367-3007-5

ISBN 978-90-367-3008-2 (electronic version)

THE PLOUGHMAN AND HIS SONS

The farmer's patient care and toil
Are oftener wanting than the soil.

A wealthy ploughman drawing near his end,
Call'd in his sons apart from every friend,
And said, 'When of your sire bereft,
The heritage our fathers left
Guard well, nor sell a single field.
A treasure in it is conceal'd:
The place, precisely, I don't know,
But industry will serve to show.
The harvest past, Time's forelock take,
And search with plough, and spade, and rake;
Turn over every inch of sod,
Nor leave unsearch'd a single clod.'
The father died. The sons—and not in vain—
Turn'd o'er the soil, and o'er again;
That year their acres bore
More grain than e'er before.
Though hidden money found they none,
Yet had their father wisely done,
To show by such a measure,
That toil itself is treasure.

Jean de la Fontaine

Cover – Front: *First image taken by the OmegaCAM Camera at the European Southern Observatory (ESO) in Garching. This acquisition has been performed by O. Iwert (Project Manager of the OmegaCAM instrument at ESO) and the Optical Detector Team members. Image Courtesy ESO.*

The work described in this thesis was performed at



Kapteyn Astronomical Institute, University of Groningen,
PO Box 800, 9700 AV Groningen, NL

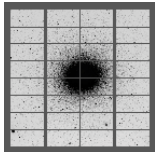


European Southern Observatory, Karl-Schwarzschild-
Strasse. 2, 85748 Garching bei München, D

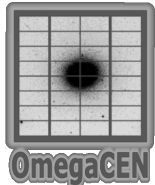
Parts of this project were funded by



Rijksuniversiteit Groningen - Kapteyn Instituut, NL



OmegaCAM Consortium



OmegaCEN - NOVA / Kapteyn Astronomical Institute,
Groningen, NL

LKBF

Leids Kerkhoven-Bosscha Fonds, NL

Printed by PrintPartners Ipskamp B.V., Enschede, The Netherlands

Copyright © F.F.T. Christen, 2007

Contents

I	Introduction	15
1	Revealing Dark Matter from Wide Field Imaging	17
1.1	Brief History of the Dark Matter	18
1.1.1	Cluster of Galaxies	18
1.1.2	Galaxies	18
1.1.3	Cosmic Microwave Background	19
1.2	Gravitational Lensing	20
1.2.1	Introduction	20
1.2.2	Basic Principles of Gravitational Lensing	20
1.2.3	Aims of Current Gravitational Lensing Programs	24
1.3	The Very Large Telescope Survey Telescope - OmegaCAM System.	25
1.3.1	The VLT Survey Telescope	25
1.3.2	The OmegaCAM Camera	25
1.3.3	Standard Filters	27
1.3.4	The OmegaCAM Shutter	27
1.3.5	OmegaCAM Instrument Software	29
1.3.6	AstroWISE	29
1.4	Outline of this Thesis	30
II	OmegaCAM CCDs Characterization	33
2	Characterization of the OmegaCAM CCDs	35
2.1	Introduction	35
2.2	The VST-OmegaCAM System: CCDs Selection	37
2.3	OmegaCAM CCD Detectors	37
2.4	Description of the Test Bench	39
2.4.1	Hardware	39
2.4.2	Software	43
2.4.3	Accessible Parameters for Standard Users	45
2.4.4	Data Produced by the FIERA Test Bench	46
2.5	CCD Test Procedure	46
2.6	Test Results	49
2.6.1	Quantum Efficiency	49

2.6.2	Photo-Response Non-Uniformity	55
2.6.3	Readout Noise	58
2.6.4	Conversion Factor	61
2.6.5	Linearity	64
2.6.6	Dark Current	67
2.6.7	Charge Transfer Efficiency	70
2.6.8	Cosmetic Defects	73
2.7	Summary and Conclusion	76
2.A	Annex A: Measurements	77
2.A.1	Quantum Efficiency	77
2.A.2	Photon-Response Non-Uniformity	80
2.A.3	Readout Noise	82
2.A.4	Conversion Factor (gain)	83
2.A.5	Linearity	84
2.A.6	Dark Current	84
2.A.7	Charge Transfer Efficiency	85
2.A.8	Cosmetic Defects	86
2.B	Annex B: Example of an ESO CCD Test Report	87
2.B.1	General Information	87
2.B.2	Volt Table	87
2.B.3	Quantum Efficiency	90
2.B.4	Quantum Efficiency, Comparison	91
2.B.5	Quantum Efficiency, Special Specification	92
2.B.6	Difference Between the QE Obtained by ESO and by e2v	92
2.B.7	PRNU Comparison	92
2.B.8	QE and PRNU Comparison of the ESO Measurements with the Specifications	93
2.B.9	Cosmetics	94
2.B.10	Cosmetic Defects	97
2.B.11	Dark and Bias Images	98
2.B.12	Readout Noise and Conversion Factor	100
2.B.13	Linearity	100
2.B.14	Dark Current	101
2.B.15	Charge Transfer Efficiency (CTE)	101
2.C	Annex C: Example of Summary Test Report	102
3	Computation of CCD Gain with TDI Images	103
3.1	Introduction	103
3.2	TDI Images, Definition and Purpose.	104
3.3	Standard Tools to Compute the Conversion Factor	105
3.3.1	Photon Transfer Curve.	105
3.3.2	Conversion Factor Determined with two Flat and two Bias Images.	106
3.4	Photon Transfer Curve from TDI Images, Gain.	106
3.4.1	Photon Transfer Curve with Two TDI Images.	107
3.4.2	Photon Transfer Curve with One TDI Image.	108
3.5	Results and Comparison.	108
3.5.1	Results	108

3.5.2	Comparison	108
3.6	Future Work	110
3.7	Conclusion	111
4	CTE from Change in Variance in Flat Field Images	113
4.1	Introduction	113
4.2	Charge Transfer Efficiency, Definition.	114
4.3	The Methods	114
4.3.1	Extended Pixel Edge Response Method	114
4.3.2	Change in Variance in Flat Field (CVF) Method	117
4.3.3	Data Acquisition and Parameter Estimation	119
4.3.4	Systematic Error Due to an Imperfect CTE, Impact on the Gain	120
4.4	Results	121
4.4.1	Simulated Data	121
4.4.2	Real Data	122
4.5	Conclusion	123
III	Gravitational Lensing	125
5	Galaxy Dark Matter Halo from 50 FORS1 Images	127
5.1	Introduction	128
5.2	Galaxy-Galaxy Lensing Theory	129
5.2.1	Galaxy-Galaxy Lensing	129
5.2.2	Definition of the Ellipticity of an Object	130
5.2.3	Distortion Matrix	131
5.2.4	KSB	132
5.2.5	Shear, Theory and Measurements	134
5.3	Models to Study the Dark Matter Halos Properties	137
5.3.1	The SIS Model	137
5.3.2	The NFW Model	140
5.4	Data Analysis, PSF Correction and Distortion Profile	142
5.4.1	Data	142
5.4.2	Stars and Galaxies Detection	143
5.4.3	Point Spread Function Correction and Shear Estimation	144
5.4.4	Object Selection	146
5.4.5	Catalog of Pairs	146
5.4.6	Tangential and Orthogonal Shear Profile	146
5.5	Results	147
5.5.1	SIS Profile	147
5.5.2	NFW Profile	158
5.6	Conclusions	166
6	Cosmic Shear Signal from Shapelets	169
6.1	Introduction	170
6.2	Description of the Data	171
6.3	Data Reduction	172
6.3.1	Data Reduction Based on the IMCAT Software and the KSB Method	172

6.3.2	Data Reduction Based on Source Extractor and the Shapelets . . .	175
6.4	Shapelets and KSB Catalogs Comparison	178
6.5	Cosmic Shear Signal Calculation	180
6.6	Analysis of Systematic Errors	183
6.7	Conclusions	186
A	Summary	188
B	Samenvatting	198
	Bibliography	208
	Acknowledgment	218

List of Figures

1.1	Geometrical construction of a typical gravitational lensing event	21
1.2	Example of a possible microlensing event in Andromeda	23
1.3	Example of strong gravitational lensing events in Abell 2218	23
1.4	The VLT Survey Telescope (VST)	26
1.5	The mosaic filled with 8 by 4 CCDs	27
1.6	Schematic view of the CCD positions in the mosaic	28
1.7	The OmegaCAM shutter	28
1.8	The OmegaCAM instrument	29
2.1	Picture of Two 44-82-1-A57 e2V CCDs	38
2.2	Overview of the test bench	40
2.3	Schematic diagram of the ESO test bench hardware setup	41
2.4	Schematic diagram of the ESO test bench software setup	44
2.5	Schematic diagram of a raw FITS image produced by the ESO test bench FIERA CCD controller	46
2.6	CCDs Position, serial number and ESO nickname in the OmegaCAM mosaic	50
2.7	QE of the 32 OmegaCAM CCDs	53
2.8	Residual QEs	54
2.9	Average, minimum and maximum QE of the 32 OmegaCAM CCDs	54
2.10	Diamond, salt and pepper and fringing pattern	56
2.11	Average, minimum and maximum PRNU of the 32 OmegaCAM CCDs	57
2.12	PRNU of the 32 OmegaCAM CCDs	57
2.13	Readout noise of the 32 OmegaCAM CCDs	60
2.14	Conversion factor of the 32 OmegaCAM CCDs	63
2.15	Example of a Time Delay Integration Image	64
2.16	Example of Linearity and Residual Linearity plots	65
2.17	Residual linearity of the 32 OmegaCAM CCDs	66
2.18	Dark current of the 32 OmegaCAM CCDs	68
2.19	Example of Charge Injection	69
2.20	Charge Transfer Efficiency of the 32 OmegaCAM CCDs	72
2.21	Cosmetic defects of the 32 OmegaCAM CCDs	75
2.22	Quantum Efficiency Curve	91
2.23	Ratio of ESO QE to Minimum Specification	91
2.24	PRNU curve	93

2.25	Image #1, 350 nm, Bandwidth 5 nm, High Gain Mode, High Level	95
2.26	Image #2, 350 nm, Bandwidth 5 nm, High Gain Mode, High Level	95
2.27	Image #1, 475 nm, Bandwidth 5 nm, High Gain Mode, High Level	95
2.28	Image #2, 475 nm, Bandwidth 5 nm, High Gain Mode, High Level	95
2.29	Image #1, 600 nm, Bandwidth 5 nm, High Gain Mode, High Level	96
2.30	Image #2, 600 nm, Bandwidth 5 nm, High Gain Mode, High Level	96
2.31	Image #1, 750 nm, Bandwidth 5 nm, High Gain Mode, High Level	96
2.32	Image #2, 750 nm, Bandwidth 5 nm, High Gain Mode, High Level	96
2.33	Image #1, 900 nm, Bandwidth 5 nm, High Gain Mode, High Level	97
2.34	Image #2, 900 nm, Bandwidth 5 nm, High Gain Mode, High Level	97
2.35	Master Bias	99
2.36	15 minutes Master Dark	99
2.37	1 Hour Master Dark	99
2.38	Linearity Error Curve	100
2.39	Residual Non-Linearity Curve	101
2.40	Summary Test Report of the CCD Sculptor.	102
3.1	Example of TDI Image	104
3.2	Typical response of a TDI image	105
3.3	Example of a noise pattern after subtraction of two TDI images	107
3.4	Example of a photon transfer curve realized with two TDI images	109
3.5	Example of non-linearity in a photon transfer curve	109
3.6	Ratio of the variance from one image to the variance from two images	111
4.1	Impact of imperfect CTE on a flat field image	115
4.2	Schematic diagram of an image with pre- and overscans	115
4.3	Signal variance versus line index	120
5.1	Example of the effect of the weak lensing by a gravitational potential	130
5.2	Illustration of the ellipticity (e_1, e_2)	131
5.3	Illustration of a gravitational lensing event	135
5.4	Selection of the source galaxies around a lens galaxy	137
5.5	Dimensionless angular-diameter distance as a function of the red-shift for two cosmological flat models, CDM and Λ -CDM	139
5.6	β parameter at different lens red-shifts for two cosmological flat models, CDM and Λ -CDM	140
5.7	Example of a (radius, magnitude) plot	144
5.8	Example of uncorrected star ellipticities	144
5.9	Illustration of the smoothing procedure of the matrix P_g	145
5.10	Illustration of the average tangential shear profile	147
5.11	Graphic representation of the average orthogonal shear profile	147
5.12	Illustration of the lens and source distribution used in this work	149
5.13	Illustration of the O. Le Fèvre data	150
5.14	Illustration of the gaussian red-shift distribution for each interval	152
5.15	Illustration of the estimate of the lens and source distribution, $F(z_l, z_s)$	152
5.16	β as a function of z_{lens} and z_{source} for the CDM model	153
5.17	β as a function of z_{lens} and z_{source} for the Λ -CDM model	153
5.18	Example of χ^2 minimization analysis	161

6.1	Example of a star ellipticity reconstruction	174
6.2	Ellipticity of the star before and after anisotropic PSF correction.	176
6.3	Ellipticity of the star before and after anisotropic PSF correction for 1/5 of the stars.	177
6.4	Slope $\alpha_{1,2}^k$ in $\tilde{\gamma}_{1,2}^{k,ksb} = \alpha_{1,2}^k \tilde{\gamma}_{1,2}^{k,shapelets}$ as a function of the seeing per each image k	179
6.5	Comparison of individual galaxy shear measurements from the KSB and shapelets pipeline	180
6.6	$\langle \gamma^2 \rangle$ with respect to the size, θ , of the top hat filter	182
6.7	Comparison of the cosmic shear signal, obtained using the shapelets pipeline, with other surveys	182
6.8	Average corrected isotropic ellipticity as a function of X and Y bands using KSB algorithm	183
6.9	Average galaxy shear estimate (from the shapelets) as a function of X and Y bands	184
6.10	Average galaxy ellipticity before and after anisotropic PSF correction as a function of the star ellipticity	185
6.11	Average galaxy ellipticity, before and after the PSF correction as a function of the star ellipticity	185
6.12	Comparison of the cosmic shear signal from shapelets to the signal from 100 set of fake data	186
1a	The Visible Universe	190
2a	The Cosmic Microwave Background	191
3a	Gravitational lensing event	192
4a	Example of an e2V44-82 CCD	193
5a	Schematic View of the Basic Layout of a Three-Phase CCD	194
6a	Schematic View of a Three-Phase CCD with Output Register	195
7a	Charge-Coupling in a Three-phase CCD	195
8a	Clock Pattern in a Three-phase CCD	195
9a	Negative Image of Mars	196
10a	Negative Image of the Galaxy NGC 4945	196
1b	Het zichtbare heelal	200
2b	De kosmische microgolf achtergrondstraling	201
3b	Zwaartekracht lens	202
4b	Voorbeeld van een e2V44-82 CCD	203
5b	Schematische weergave van de opbouw van een driefase-CCD	204
6b	Schematische weergave van een driefase-CCD met uitgangsregister	205
7b	Charge-Coupling in een driefase-CCD	205
8b	Klopatroon in een driefase-CCD	205
9b	Negatieve opname van Mars	206
10b	Negatieve opname van het NGC 4945 stelsel	206

List of Tables

2.1	Statistical analysis of the readout noise	59
2.2	Statistical analysis of the conversion factor	62
2.3	Statistical analysis of the linearity	66
2.4	Statistical analysis of the dark current	68
2.5	Statistical analysis of the charge transfer efficiency	71
2.6	Statistical analysis of each cosmetic defect	75
2.7	QE measurements of the 32 OmegaCAM CCDs	79
2.8	PRNU measurements of the 32 OmegaCAM CCDs	81
2.9	Readout noise measurements of the 32 OmegaCAM CCDs	82
2.10	Conversion factor measurements of the 32 OmegaCAM CCDs	83
2.11	Non linearity measurements of the 32 OmegaCAM CCDs	84
2.12	Dark current measurements of the 32 OmegaCAM CCDs	84
2.13	Charge transfer efficiency measurements of the 32 OmegaCAM CCDs	85
2.14	Cosmetic defects measurements of the 32 OmegaCAM CCDs	86
3.1	Conversion factor measurement of 7 CCDs using different methods	110
4.1	Theoretical estimate of the gain's error due to an imperfect CTE	121
4.2	CVF method applied on simulated data to estimate the CTEs of the CCDs	122
4.3	Impact of an imperfect CTE on the gain	122
4.4	Horizontal and Vertical CTE of 9 CCDs using different methods	124
5.1	Reproduction of the data from Le Fevre et al	150
5.2	Estimation of z_m and σ for the gaussian redshift distribution	151
5.3	Average and characteristic velocity dispersion for different cosmological models	157
5.4	Estimate of parameters which characterize a galaxy at a reference luminosity L^* using the NFW profile and the CDM model ($\Omega = 1$)	162
5.5	Estimate of parameters which characterize a galaxy at a reference luminosity L^* using the NFW profile and the Λ -CDM model	163

